Miniaturized Differential Dual Circularly Polarized Traveling Wave Dielectric Resonator Antenna Array with High Ports Isolation

Yazeed Qasaymeh[1*], Mohammad Alibakhshikenari[2,3*†], Omar Alharbi[1†], Jaume Anguera[4†], Isabelle Huynen[5†], Iyad Dayoub[6,7†], Takfarinas Saber[2†], Ernesto Limiti[8†], Abdullah Almuhaisen[1†]

[1*]Department of Electrical Engineering, College of Engineering, Majmaah University, Al-Majmaah, 11952, Saudi Arabia.
[2]LERO, the Research Ireland Centre for Software College of Science and Engineering, School of Computer Science, University of Galway, Galway, H91 TK33, Ireland.
[3]Department of Electrical and Electronics Engineering , Dogus University, Istanbul, 34775 Umraniye, Turkiye.
[4]Research Group on Smart Society, La Salle Engineering, Universitat Romon Llull, Barcelona, 08022, Spain.
[5]ICTEAM Institute, Universite Catholique de Louvain, Louvain-La-Neuve, 1348, Belgium.
[6]IEMN, Institut d'Electronique, de Microctronique et de Nanotechnologie, UMR CNRS 8520 University Polytechnic Hauts-De-France, Universitlytechnique, Valenciennes59300, France.
[7]INSA Institut National des Sciences Appliqu Hauts-de-France Valenciennes59300, France.
[8]Electronics Engineering Department, University of Rome Tor Vergata, Rome, 00133 Rome, Italy.

*Corresponding author(s). E-mail(s): y.qasaymeh@mu.edu.sa; mohammad.alibakhshikenari@universityofgalway.ie;
Contributing authors: oalharbi@mu.edu.sa; jaume.anguera@salle.url.edu; jaume.anguera@salle.url.edu;

iyad.doyoub@uphf.fr ; takfarinas.saber@universityofgalway.ie;
limiti@ing.uniroma2.it; a.almuhaisen@mu.edu.sa;
†These authors contributed equally to this work.

Abstract

The current study presents a differential traveling wave series fed dielectric resonator antenna (DRA) array with dual circularly polarized (DCP) operating for IEEE 802.11a applications. To possess circular polarization (CP) fields, a unique antenna element composed of rectangular dielectric resonators (RDR) coupled with octagonal slots (OS) at the ground plane and excited by the mean of a microstrip feed at the front plane is proposed. The proposed resonating element generates two orthogonal modes, $\boldsymbol{TE^{x}_{\delta 21}}$ and $\boldsymbol{TE^{y}{}_{1\delta 1}}$, ensuring the existence of CP performance. To obtain a DCP performance, the proposed resonator is utilized for portraying a seven-element array employing a concentric ring fed with dual differential port excitation. The concentric ring fed allows choosing the direction of the input wave and, accordingly, the orientation of the CP. Hence, synchronous feeding to both ports yields in generating waves of various polarization states. The $\mathbf{50 \times 50}$ $\mathrm{mm}^{\mathbf{2}}$ array exhibits an resonance bandwidth of 12.15% with an polarization purity of 12.5%. Meanwhile, the inter-port isolation varies from -18 dB to -39 dB along the resonance band. The realized measured gain ranges from 11.33 to 12.44 dBi. The proposed array exhibits DCP capability, and therefore it fits for various applications.

Keywords: Concentric ring fed, Dielectric resonator antenna, Dual circular polarization, Miniaturized, Ports isolation, Wideband

1 Introduction

Due to its striking characteristics, such as compactness, lightweight, high radiation efficiency, minimal losses, extensive bandwidth, and no excitation of surface waves, the DRA has wide use in millimeter-wave applications. Another important feature is that it can be excited with various coupling methods such as slot coupling [1], microstrip coupling [2], image guide coupling [3], and coaxial probe coupling [4]. One more key characteristic of DRA is that the DR can be shaped into different forms such as cylindrical, hemispherical, and rectangular [5]. More importantly, it can be formed into an array, which can provide a DCP performance.

In fully polarized wireless systems such as radar and navigation, the DCP antenna is a crucial element. This is mainly attributed to the ability of DCP antennas to increase the capacity of wireless systems due to their appealing characteristics of opposing the multi-path fading effect [6]. The communications channels utilizing DCP antennas for high capacity require a high port isolation. The port isolation and high bandwidth are vital factors affecting the simplicity of the receiver design as self-interference cancellation requirement will be less at the receiver stage [7].

For dual-polarized (DP) performance, few DRA array designs were presented in the literature. Numerous designs were introduced in the literature for DP DRA using coupling slots. This technique attracted many researchers because the port isolation is further enhanced with the employment of coupling slots [9]. Gao and Luk (2003) [10] indicated a dual linear polarized (DLP) single-element DRA. The design utilizes two orthogonal microstrips fed to excite a cylindrical DR. The 200×150 mm^2 achieves a bandwidth of 12% and 13% for each polarization state with port isolation of about 35 dB. However, the gain performance was weak, as a single element is utilized, of about 5 dBi. The design was bulky, and the gain performance was low. Tang et al. (2009) [11] presented a hybrid differential feeding topology to obtain DLP performance. The design employs a horizontal coupling of an H-shaped slot and vertical ports coupling a balancing slot to excite a single cylindrical DR. The 54×54 mm^2 operates at the C-band with an resonance bandwidth of 7.9% for the horizontal port and 11.9% for the vertical port. Moreover, the isolation between the ports was 35.9 dB with a realized gain of about 6.8 dBi. Gau et al. (2014) [12] demonstrated a DLP single-element DRA. The design geometry is composed of bowtie-shaped slots coupling an RDR and excited by two differential orthogonal feds to trigger DLP. The antenna achieves 30.34% and 26.73% for ports 1 and 2, respectively, with a peak gain of 6.65 dBi and port isolation of 39.93 dB. Sun et al. (2013) [13] reported a DLP single-element DRA using a slot-metallic strip fed by two differential orthogonal microstrip feds to functions in the S-band. The 150×150 mm^2 attains a DLP and dual operating bands for each port. The impedance bandwidth within the S-band was 39.51% and 31.71% for ports 1 and 2, respectively. The peak gain was 8.98 dBi and a 36 dB as ports isolation.

Very few DP DRA arrays were presented. Rana and Parui (2016) [14] presented a 4×1 array with size of 135×85 mm^2 operating within the range 6.27 to 6.87 GHz and a maximum realized gain of 11.8 dBi. By triggering the array with two deferentially orthogonal feds DLP resonance was attained with 36 dB as ports isolation. Moreover, Dwivedy et al. (2018) [15] presented a DLP using two differential feeding orthogonal ports array with size of 190×82 mm^2 with 2×1 topology operating within 6.0 to 6.6 GHz. A 12.5 dBi was realized as the peak gain. A DLP DRA array multilayer 2×2 operating at a center frequency of 28 GHz reported by Kowalewski et al. (2020) [16]. The array is composed of RDR mounted above cross-shaped slot. With the use of two perpendicular feds, the array emits DP patterns. An The 35×35 mm^2 of 2×2 interlaced SR array was presented by Qasaymeh (2022) [16]. The array is consists of four resonating elements each is made of a RDR placed above and eye-shaped slot whist the CP orientation is controlled by two differential interlaced feds. The impedance bandwidth for LHCP was 2.48% if excited by port 1 and 2.28% for RHCP if excited by port 2.Yousfi et al (2024) [17] reported 3×4 DLP DRA aaray. The DP is obtained by proposing a cross-notched DRA and the polarization reconfigurability is achieved through two differential ports. The $0.2\lambda \times 0.2\lambda$ exhibits an impedance bandwidth of 13.3% with ports isolation of 17 dB and gain about 7 dB. Ma et al (2024) [18] proposed a dual-polarized meta-dielectric resonator antenna array. the 2×2 array was excited by two ports, one for vertical polarization and other for horizontal polarization. The 340×340 ^{2} antenna achieves a bandwidth of 57.4% (7.44 GHz to

13.44 GHz) for the H-polarization and 57.7% (7.41 GHz to 13.43 GHz) for the V-polarization. The ports isolation was about 29.5 dB and the gain varies from 10.5-11.1 dBi. The array suffers of design complexity as well as a bulky size. Fan et al (2026)[19] presented a dual-polarized stacked dielectric resonator antenna array operating in the 6G band (7.125?8.4 GHz). The 2×2 consists of four elements each is made of three dielectric resonators (DRs) stacked in ascending permittivity. The 60×60 mm^2 obtains a resonance frequency of he frequency range of 7.1?8.4 GHz with peak gain of 5.7 dBi and ports isolation less than 17 dB. As can be seen in the presented literature, the designs suffer from either low gain, large size, low port isolation, or dissimilarity, which are major drawbacks. Hence, the proposed design has to overcome these limitations in terms of compactness versus gain enhancement, high ports isolation versus design simplicity and similarity between polarization states versus the feeding geometry.

The phenomena of attaining a DCP is not deeply investigated. Hence, in the current manuscript, an effort to introduce a DCP DRA array is exerted aiming to attain a compact size, wideband resonance, good port isolation, and acceptable gain magnitude. Moreover, the theoretical analysis of concentric ring fed DRA array for DCP performance with uniform radiation element is presented. The goals of this manuscript are threefold. Proposing a unique CP antenna element consists of an RDR coupled with an OS is the first goal of this study. The second objective is to employ the proposed resonating element in designing DCP DRA array acquiring some bandwidth and gain enhancement, overall size reduction, and attaining good port isolation. Providing a full description of the power flow over the array and the contribution of each array element is the third goal.

The subsections of the manuscript are organized as follows. In Section 2, a novel CP resonating element, consists of an OS triggering a RDR, is suggested and parametrically studied for validation. The section ends by describing the geometry of concentric ring feeder utilized to portray a differential DCP array. Section 3 demonstrates a mathematical representation governing the power flow all over the initiated array. Results and discussions are drawn in Section 4. Lastly, the conclusion is discussed in Section 5.

2 Array Geometry

2.1 Resonating Element

Figure 1 portrays a three-dimensional geometry of single resonator element composed of an OS triggering an RDR at the bottom side and fed by a microstrip line at the front side The microstrip slot couple was first reported by Pozar (1985) [20]. Since then, this coupling schematic has been intensively used in designing DRA due to its several appealing features such as having the feed network situated underneath the bottom plane, hence eluding inauthentic and degeneracy radiation, ensuring that the DRA emits most of the energy. Furthermore, in the array applications, it makes the entire bottom surface available for the radiating elements only. OS shape is utilized in this design as its compacted architect comprises more area coverage compared to typical triangle or circle slot shapes. Octagonal slot offer superior impedance matching, wider bandwidth especially for ultra-wideband applications, and smoother current distribution. By avoiding the sharp corners of rectangular slots and the abrupt current concentrations of circular slots, the octagonal shape reduces signal reflections and lowers cross-polarization [21]. One more major advantage of using the coupling slot is that due to the high amount of coupling, the port isolation will be reduced, yielding the diversity of the DR overall performance.

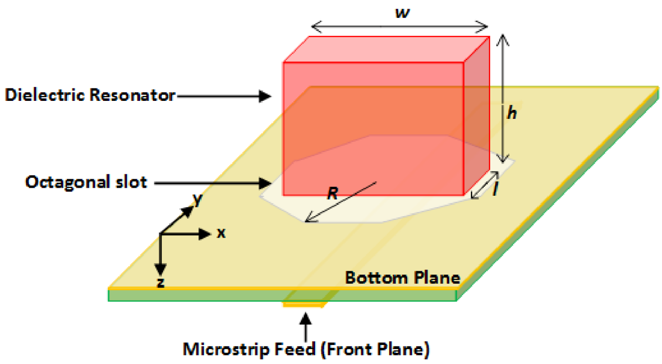

Fig. 1 3D representation of the proposed single-element resonator

The DR rectangular geometry is utilized in this design as it has a main advantage; that is, its geometrical dimensions L, W, and H can be characterized independently. Hence, compared to other conventional DR shapes, more design flexibility is offered. Furthermore, the rectangular DRA offers low cross-polarization level as compared to the other DRA architectures [22]. Furthermore, in the case of RDR, the mode degeneracy can be avoided by appropriately adjust the three dimensions compared to spherical DRA where the mode degeneracy permanently occurs and hybrid modes for the cylindrical DRA [22]. The dielectric waveguide model is utilized for synthesizing the RDR geometry. If the DR is positioned over the ground plane, TE modes are generated. Meanwhile, for the TE^x_{111} mode, the resonant frequency is estimated using Equation (1).

The dielectric waveguide model [23,24] is utilized for synthesizing the RDR geometry. If the DR is positioned over the ground plane, TE modes are generated. Meanwhile, for the TE^x_{111}, the resonant frequency is estimated using Equation (1) as follows:

$$f_0 = \frac{c}{2\pi\sqrt{\epsilon_r}}\sqrt{k_x^2 + k_y^2 + k_x^2}. \tag{1}$$

where k_0 is the wave number of free space,c is the light velocity, and k_x, k_y, and k_z are the wave numbers in the x, y, and z directions within the RDR boundaries, correspondingly.

The OS radius R can be estimated using Equations (2) and (3) reported by [25,26] as follows

$$F = \frac{8.791 \times 10^9}{f_r\sqrt{\epsilon_r}}. \tag{2}$$

$$R = \frac{F}{\left(\left[1+\frac{2h}{\pi\varepsilon_r F}\right]\left[\ln\left(\frac{\pi F}{2h}+1.7726\right)\right]\right)^{0.5}}. \quad (3)$$

where h is the substrate thickness, ϵ_r is the dielectric constant.

2.2 Single-Element Parametric Study

In this part, the proposed novel resonating element is investigated to authenticate the proposed hypothesis of obtaining a novel compact resonating element that can generate CP patterns. Thus, a single resonating element as shown in Figure 2 is modelled using Computer Simulation Technology (CST) microwave studio. In Figure 2(a) the microstrip feed is carved on the front plane of RO4003C laminate from Rogers. Meanwhile, in Figure 2(b) the OS carved on the bottom plane is shown. Finally, in Figure 2(c), the RDR made of alumina material of dielectric constant which is equal to 10 is mounted above the OS.

Figure 3 depicts the effect of altering the antenna sub-elements on the resonance frequency with an intended design frequency of 5.8 GHz. The figure illustrates various parametric sweeps of the RDR width and length while setting the OS side fixed at 3 mm. In Figure 3(a), the effect of altering the RDR on the resonance frequency is demonstrated while maintaining both the height and width maintained at 5 mm. Form figure, its observed that if the length increases, the resonance frequency shifts to the left with more matching. In addition, similar results are obtained in Figure 3(b), which depicts the width variation effect on resonance frequency. In Figure 3(c), the RDR height effect on the resonant frequency is plotted. Possible to observe that if the RDR height increases, the operating frequency shifts to the left. Hence, it can be inferred that the optimum resonance takes place at 5.8 GHz if the width, length, and height of the RDR are 5 mm while maintaining the OS side settled at 3 mm.

Once the resonant frequency is fine-tuned, the resonating modes need to be determined. To obtain a CP attitude, two perpendicular modes need to be generated inside the RDR boundaries. Hence, the electric field distribution inside the RDR boundaries must be justified. Therefore, Figure 4 depicts the electric field lines distribution in the xz and yz planes. The field lines distributions demonstrate that the two orthogonal modes $TE^x_{\delta 21}$ and $TE^y_{1\delta 1}$ generated

Figure 5 illustrates the Smith chart of the proposed resonator at the optimal resonance frequency. Two significant observations can be noticed from the figure. Firstly, the tiny loop at the center of the chart ensures the presence of CP radiation. Secondly, a good matching is obtained as the marker indicates 49 Ω

The AR alterations in line with the RDR dimensions are shown in Figure 6. In Figure 6.a presents the AR performance versus the width and length of the RDR and Fiure 6.b depicts the AR variation in accordance to OS side length The results coincide with the results of Figures 3(a) and 3(b) that once the dimension increases, the performance goes to lower frequencies and the polarization purity decreases.

Figure 7 depicts the three-dimensional radiation pattern of the optimized resonator. A few things are observed from the figure. Firstly, a directive radiation pattern is attained. Secondly, the radiation pattern is mainly from the RDR, and it is minimal

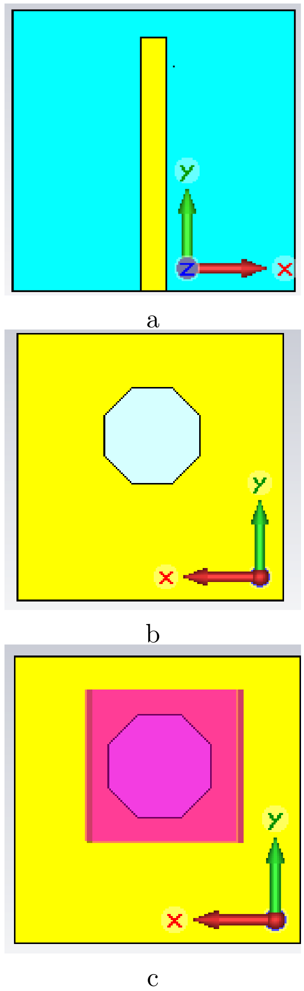

Fig. 2 Proposed resonating element modelled using CST: (a) Front plane showing the microstrip fed; (b) Ground plane displaying the OS; (c) Ground plane displaying the RDR located above the OS

in the side of the microstrip fed. Finally, an excellent gain is achieved. As can be seen from the figure, 6.54 dBi is obtained as normally a single RDR scores about 5 dBi

2.3 Array Configuration

The array networks can be classified into two types of topologies: the series and parallel fed arrays. For parallel geometry, the long lines causes high losses and hence affect the array gain performance [26]. Also, the achievement of DCP utilizing the parallel-fed geometry yields a complex design. For the series fed geometry, improving the array efficiency is feasible at the expense of increasing the array elements number yielding a bulky array size [27]. Whilst, the series-fed topology cannot possess DCP radiation due to its symmetry. For that, a dual port feeding for a circular concentric ring allows

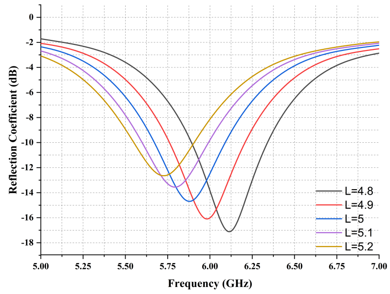

a

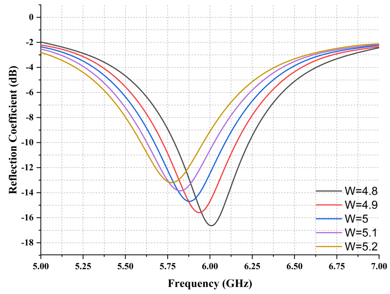

b

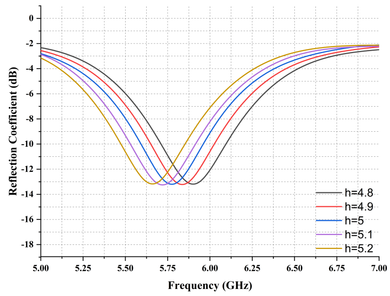

c

Fig. 3 Parametric sweep of the RDR effect on the resonant frequency corresponding to RDR dimensions: (a) The length of the RDR; (b) The width of the RDR; (c) The height of the RDR

controlling the sense of the polarization direction. In other words, synchronous feeding to both ports can result in radiating waves of arbitrary polarization. The DCP antennas can be classified into two main kinds: differential fed [28] and commonly fed antennas [29]. The commonly fed antennas involve the integration of RF switches to alter the polarization resulting in a more design complexity. One more disadvantage is the delay in switching between the polarization states. For the previously mentioned reasons, the differentially fed antennas are more convenient in designing antennas for DCP performance.

Figure 8 illustrates the proposed DCP array archetype. The feeding microstrip geometry on the array front plane is illustrated in Figure 8(a). Meanwhile, the allocation of the resonating elements is shown in Figure 8(b). In the front plane, the feeding

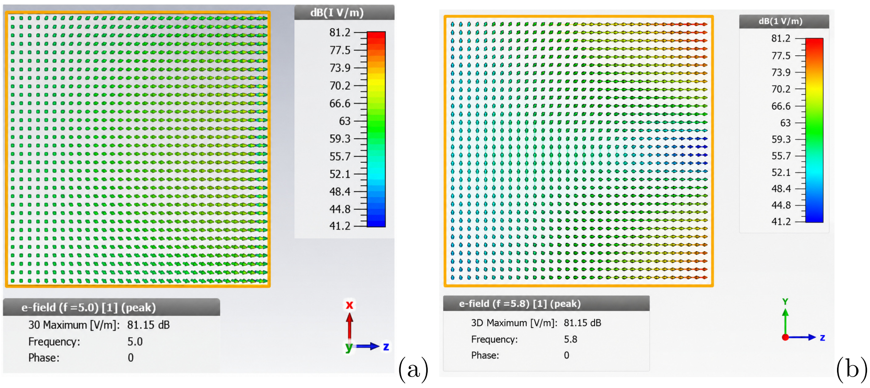

Fig. 4 The electric field lines distribution within the RDR: (a) The xz plan; (b) The yz plan

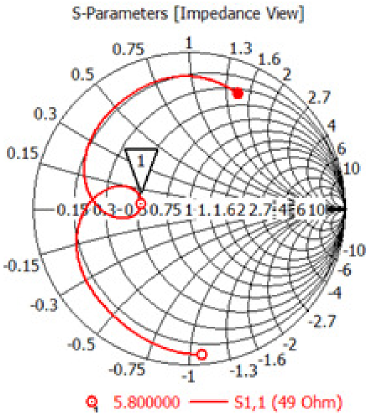

Fig. 5 The Smith chart of the optimized resonating element

topology is composed of a circular concentric ring with two feeding ports allowing for DCP. For the coupled power from the feeding network to be maximum, the resonating elements are spaced a wavelength apart. Hence, the feeder circumference measures about 112.48 mm. As the laminate RO4003C from Rodgers is to be used in fabrication, at 5.8 GHz. It worth to mention that, for arrays with elements spaced $< \lambda/2$ have higher mutual coupling with grating lobes are eliminated. Whilst, for elements spaced $> \lambda/2$, brings severe grating lobes and reduce the mutual coupling.

The array has two ports situated between the elements 1 and n. If the two ports are trigged, correspondingly, the current in the feeding network is reversed. Hence, a dual CP is achieved. To allow for DCP performance, the concentric ring microstrip feed is excited from port 1, and it is expected to produce a RHCP. Meanwhile, a LHCP is expected if the concentric ring fed is excited at port 2. Hence, DCP radiation can be generated by feeding both ports. As seven resonating elements are to be evenly placed in accordance with the z-axis, the current phase shift progression is to be 45^0 from one element to another. The phase shifting for the first element is 45^0, and the phase increment is 45^0 from one radiating element to another along the feeder. One more

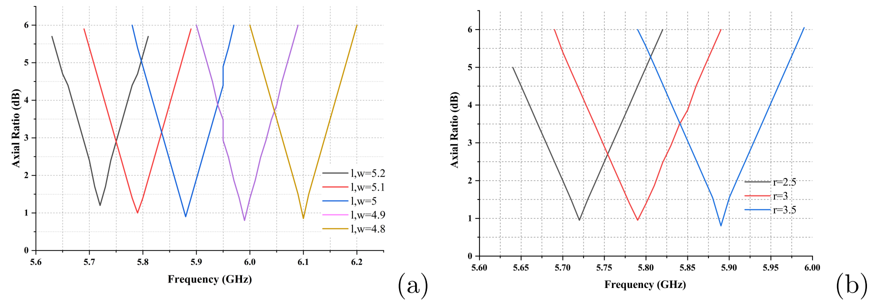

Fig. 6 (a) The AR variations in accordance with the RDR dimensions; (b)The AR variations in accordance with OS side length

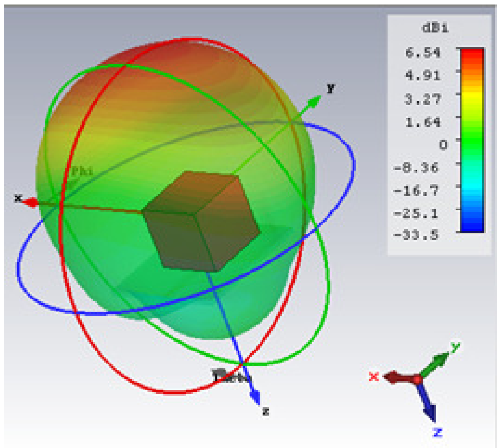

Fig. 7 3D radiation pattern of the proposed resonating element

advantage of the proposed coupling method is its symmetry. Therefore, a symmetric radiation pattern is to be achieved, and that would help in improving polarization purity. Moreover, due to the array symmetry with respect to the feeding ports, a high quality of CP is acquired.

3 Theoretical Investigation

3.1 Power Flow Analysis

The individual radiating elements are progressively coupled to possess a segment of the power of the traveling wave from one port to another. Even though the radiating elements are equally coupled, the strength of the coupling power decreases over the feeding line. The field flowing over the microstrip fed will induce a magnetic field within each coupling slot, and some of the energy is to be coupled with the radiating elements from the fed line. As the power is coupled by the fed line through the aperture, it is expected that less power will remain for the remaining array elements. To explain the power flow over the array, Figure 9 depicts the radiation model for a single array

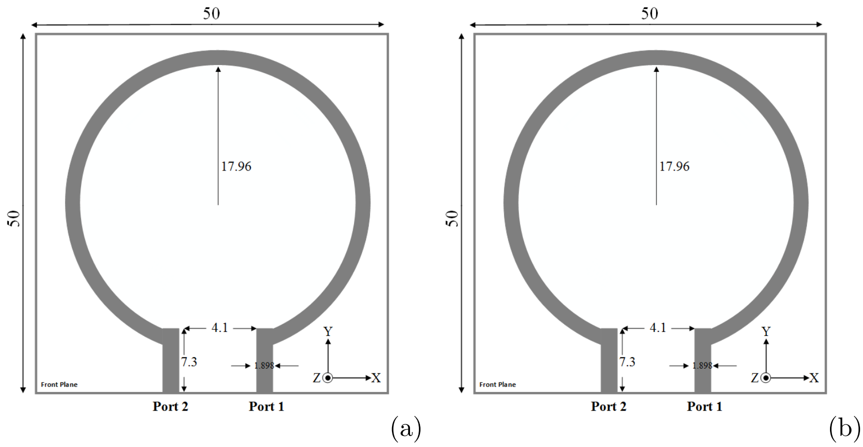

Fig. 8 Geometry of the proposed dual-polarized array: (a) Front plane; (b) Ground plane

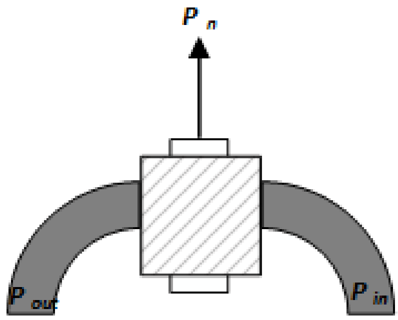

Fig. 9 Power allocation for a single radiating element

element. For any element n of the array, the radiated power is denoted as P_n , where P_{in} denotes the input power of the element and P_{out} denotes the power still progression on the line leaving to couple the next array element.

If a uniform array element is fed by a traveling wave microstrip, the power received from the ports is successively distributed. Hence, the power continually triggers the radiating elements. The power radiated by the element n can be expressed as in Equation (4) reported by [30]:

$$P_n = (1 - \alpha)^{n-1}\alpha. \tag{4}$$

where α is the coupling coefficient and defined as $\alpha = ((1 - |S_{11}|^2 - |S_{21}|^2))?((1 - |S_{11}|^2))$ where S_{11} and S_{21} represent the reflection coefficient and transmission coefficient, respectively. n is the number of the array elements [30].

It can be extracted from Equation (4) that if the array is formed of uniform elements and with uniform elements-spacing, the power coupled with each array element along the microstrip fed will be equal and hence approximately equivalent power to radiate from all the elements. The array over all radiated power can be estimated using Equation (5) documented in [31]:

$$A = \sum_{n=1}^{N} P_n = 1 - (1-\alpha)^n \tag{5}$$

To obtain an adequate coupling power to the radiating elements, a sufficient current needs to be delivered to the radiating elements. Figure 10 depicts the current distribution over the feeding ring microstrip once it is fed by port 1 as in Figure 10(a) and if it is fed by port 2 as in Figure 10(b) using Computer Simulation Technology (CST) microwave studio software. In both cases, it can be concluded that the current is maximum (node) approximate over the coupling slots at the ground side. The result coincides with the assumption that the SWR will repeat itself every wavelength over an open-ended microstrip. The CP direction whether a RHCP or LHCP can be judged by tracking the surface current progression phase from one element to another starting from the excitation source. In Figure 10, where the resonating elements are triggered by port 1, the current phase progression from one element to another is in a clockwise direction. That is, RHCP radiation is obtained. Meanwhile, if the radiation elements are excited by port 2, the surface current phase progression from one element to another is counter-clockwise. That is, a LHCP is attained. Hence, a DCP radiation is acquired using the same radiation elements utilizing the same feeding network.For both cases, as can be noticed from Figure 10,equal phase progression is obtained due to uniform element spacing. As a consequence of that, a uniform power coupling and negligible reflections is expected.

Figures 11 and 12 depict the power allocation over the prototyped design once the array is excited from port 1 and port 2, respectively. From the figures, it can be observed that the power is distributed evenly between the coupling slots. The result agrees with the assumption made in Section 2 that the nodes are to be repeated every wavelength. Also, the figures reveals that the array elements will contribute almost evenly to the array radiated power. Furthermore, it can be observed that; due to array elements accurate allocation and consistent spacing, a uniform coupling magnitude is obtained along the feeding network. In accordance with this result, the power coupling of the RDR is adequate, and hence the array radiated power is to be optimal. Consequently, the array gain performance is to be optimal.

3.2 Mathematical Insight

For communication links with high capacity, DCP antennas are preferred to have high port-to-port isolation. This characteristic is important in polarimetric applications which requires small mutual antenna ports coupling between to have a better accuracy and simplify receiver design. The ports isolation can be estimated using Equation (6) [33]

$$S_{21} = -log_{10}(1 - A) \tag{6}$$

From Equation (6), it can be observed that the ports isolation is dependent on coupling coefficient α and array elements number N. Figure 13 depicts the relationship

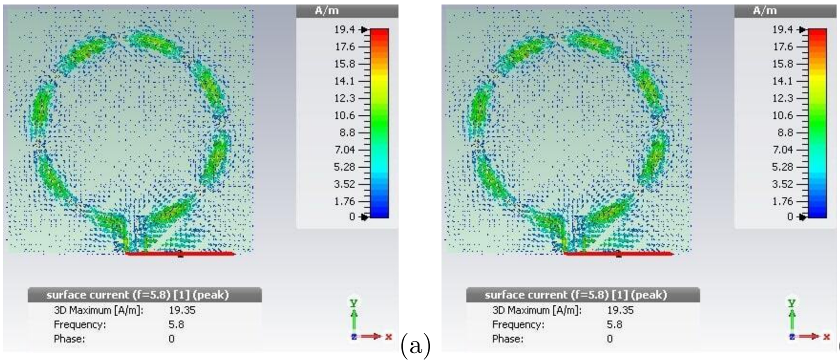

Fig. 10 Current distribution over the feeding network once it is fed by: (a) port 1; (b) port 2

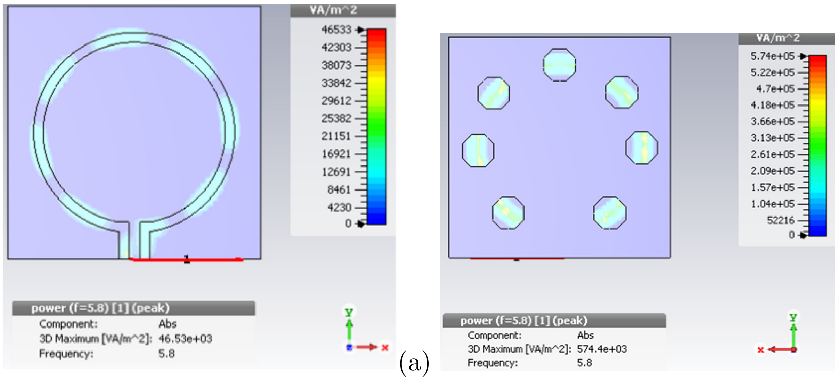

Fig. 11 Power allocation over the feeding network once the array excited by port 1 at: (a) front plane; (b) bottom plane

between the ports isolation versus the coupling coefficient and array elements number. It can be observed from figure that the ports isolation increases once the coupling and number of elements increase. The coupling coefficient is effected by the scattering. Whilst, for the array elements number effect, a trade-off between the array size and antenna performance needs to be considered.

For more understanding of the relation between the coupling coefficient and total radiated power, Figure 14 depicts a parametric study for different cases of coupling coefficient and array elements number. It can be seen from figure that when the array elements number increases, more total radiated power is obtained. For example if $\alpha=$ 0.57. Consequently, for the array fifth element, the associated power is 0.987 which infers that the first five array elements provide with 98.7% of the total power radiated by the array. Identical outcomes are attained once port 2 is triggered.

4 Results and Discussion

To validate the anticipated design, an antenna model is fabricated for experimental characterization. The antenna substrate was fabricated using the laminate RO4003C

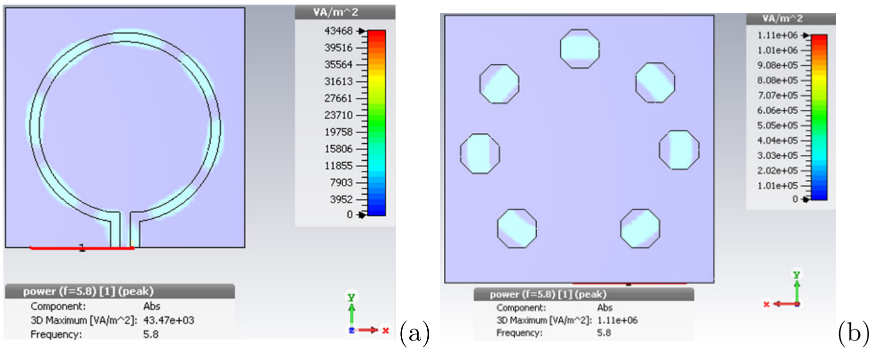

Fig. 12 Power allocation over the feeding network once the array excited by port 2 at: (a) front plane; (b) bottom plane

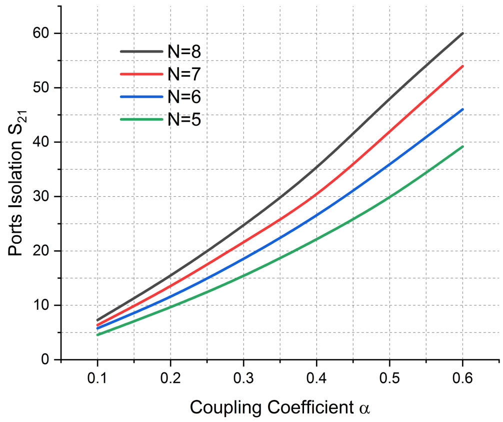

Fig. 13 Ports isolation relation with coupling coefficient and array elements number.

from Rogers with a permittivity of 3.38.. The Alumina material with permittivity of 9.8 RDR is used to model the RDR. The dimensions of the RDR and the OS are as described in Section 2.1. On the front side, the microstrip feed is etched, whereas the OS is carved on the ground plane. The geometry of dual polarization feeding and the octagonal slot allocation is as described in Section 2.3. Figure 15. depicts the fabricated array showing the feeding network on the front side and the RDRs coupled with the OSs on the ground sided. For mechanical stability and sselmbly challenges, the PCB was assembled by PCBgogo company, Whist, the DRs were mounted above the OS using Epoxy

The measurement environment setup is shown in Figure 16. The return loss measurement is executed using VNA-0460 from MegIQ. Whilst, the radiation pattern measurement is performed in anechoic chamber by keeping the distance between the

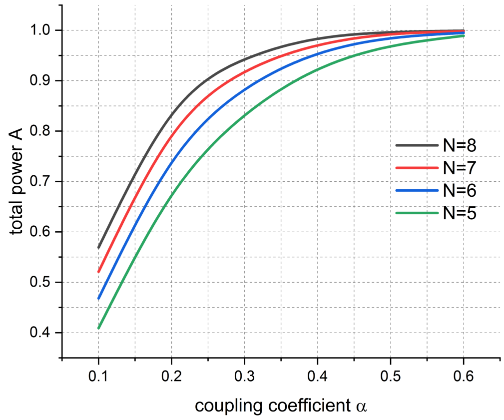

Fig. 14 Radiated power relation with coupling coefficient and array elements number .

AUT and the standard antenna satisfying the far field requirement. The signal generator SG6000X from DSI and RSA2000X from SPECTRAN were used to conduct the measurements.

Figure 17 depicts the reflection (S_{11}) and transmission (S_{21}) coefficients for both simulation and measurements. The array operation bandwidths for reflection and transmission are considered once they are below S_{11} < -10 dB and S_{21} < -15 dB, respectively. A decent accord among the simulation and measurement results was noticed. The simulated resonance bandwidth was 12.19% extends from 5.222 to 5.9 GHz with optimal matching occurring at 5.802 GHz of -32.15 dB. Meanwhile, the measured impedance bandwidth was 12.15% extending from 5.224 and ending at 5.9 GHz with minimal resonance take place at 5.792 GHz of -28.87 dB. Also, the port isolation remains below -15 dB along the operation band as indicated by the S_{21} curve, implying sufficient port isolation. The ports isolation is ideal at frequencies near to the optimal design frequency of 5.8 Ghz. Hence, the suggested array is applicable for systems implying DCP. Applying reciprocity, the proposed array might be utilized for polarimetric detection as it splits the waves upon its CP components.

Figure 18 depicts the radiation patterns in the xz for simulation and measurement 5.8 GHz if the array is triggered with one port and the other port is ceased. As can be seen from the figure, the array emits an LHCP once triggered by port 2 and an RHCP if excited by port 1. The agreement between the simulation and measured results was in good. This is mainly ascribed to the precision of setting the simulation and measurement environment. Furthermore, additional main advantage can be noticed from the radiation pattern; that is, a directive pattern is achieved. This is mainly ascribed to the even distribution of the array elements around the z-axis in circular manner.For both polarization states, the cross-polarization levels remains lower than the co-polarized ones among the operation bandwidth. Due to array symmetrical feeding topology, the radiation pattern remains balance

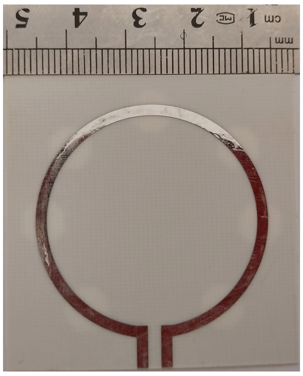

a

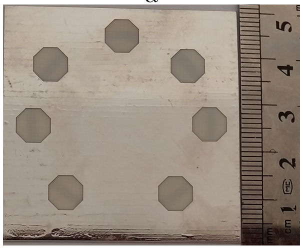

b

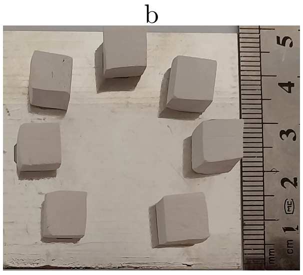

c

Fig. 15 The fabricated array: (a) Front view showing the concentric fed network; (b) Bottom view showing the OSs allocation; (c) Bottom view showing the RDR mounted above the OSs

Figure 19 depicts the phase difference vs theta. The figure reveals that there are two orthoonal electric field componenets are 90^0 apart . Figure 20.a depicts the simulation and measurement results for both boresight AR and realized gain. The simulated and measured AR results were consistent. The simulated and measured 3-dB AR bandwidths were 13.45% and 12.5%, respectively, covering the antenna operation band. For the realized gains, a good correspondence between the simulation and measurement is observed. The measured realized gain is maintained between 11.33 and 12.43 dBi within the operation band. A small variance between simulated and measured gains might be attributed to measurement imperfection. Meanwhile, the simulated radiation efficiency for both polarization states ranges from 83% and 85% . Figure 20.b depicts the simulated gain for different array elements number for operation band for each case. The figure shows that the gain increases gradually as the elements number increases.

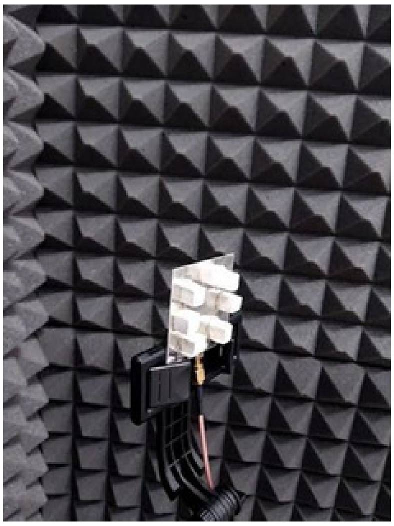

Fig. 16 Measurement setup

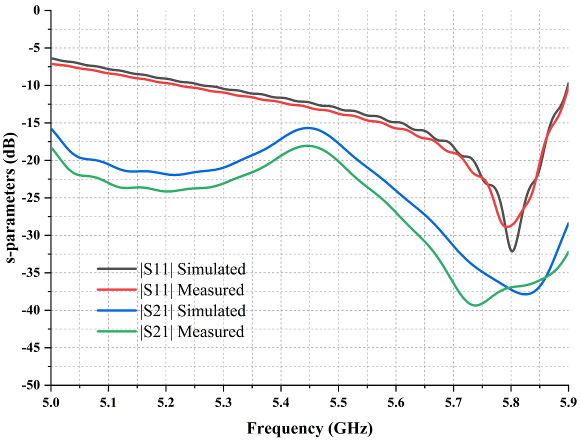

Fig. 17 Simulated and measured reflection and transmission coefficients

5 Conclusion

A DCP traveling wave series fed DRA array operating in the IEEE.802.11a has been designed and experimentally examined. The array is made of a novel resonating element whose geometry is described as an OS coupling an RDR. The proposed resonating element emits the modes $TE^{x}_{\delta 21}$ and $TE^{y}_{1\delta 1}$, ensuring the existence of CP radiation. The compact array of 50×50 mm^2 achieves an impedance bandwidth of 12.15% for both polarization states. The realized gain ranges from 11.33 to 12.44 dBi with 12.5% AR polarization purity. Moreover, good port isolation of 39 dB was achieved. Table 1 compares the proposed design with other DP DRA arrays in terms of DP technique,

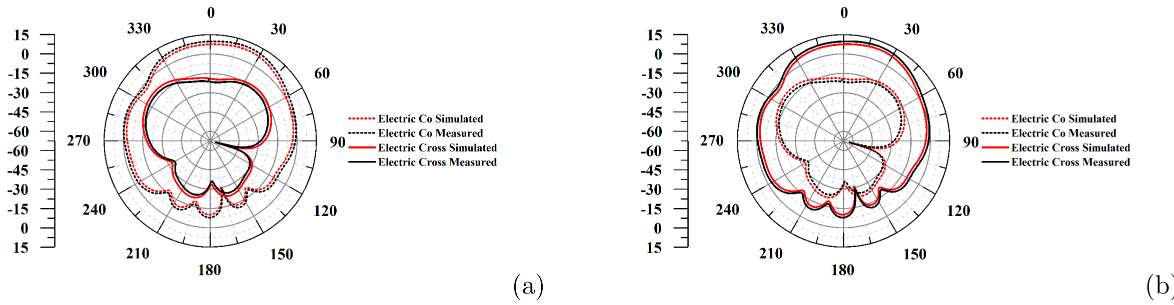

Fig. 18 Simulated and measured 5.8 GHz radiation patterns in the xz plane of the array once excited by one port and the other is terminated: (a) Excited by port 1; (b) Excited by port 2

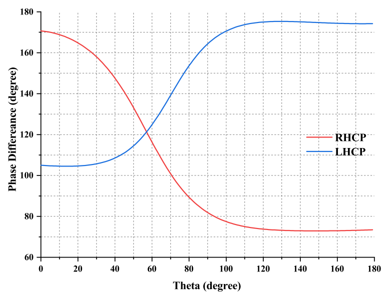

Fig. 19 Phase difference between RHCP and LHCP at 5.8 GHz

impedance bandwidth, port isolation, gain, and overall size. Compared to the DP DRA designs presented in the table, an acceptable trade-off between antenna parameters can be noticed in the proposed array. As can be seen in Table 1, an acceptable trade-off between the design complexity and size reduction to obtain a DCP performance. A potential applications for proposed design might include ISM applications, Network access points, WiFi and Wireless LAN applications, Radio local area networks, WiMAX networks, wireless audio, and video system. For future work, the number of array elements can be increased, and the same design concept can be applied to different wireless standards. Furthermore, The presented design can be tuned to operate at other freqeuncy bands such as Ultra Wide-band UWB as in [33] or mid-5G as in [34] by taking into account the physical spacing between the array elements, the dimension of each the OS and RDR. Also, the presented design can be utilized in MIMO systems depending on the signal polarization sense or employing suitable modulation scheme.

Declarations

- Funding: The authors extends their appreciation to the Deanship of Postgraduate Studies and Scientific Research at Majmaah University for funding this research work through the project number ICR-2026-xxx

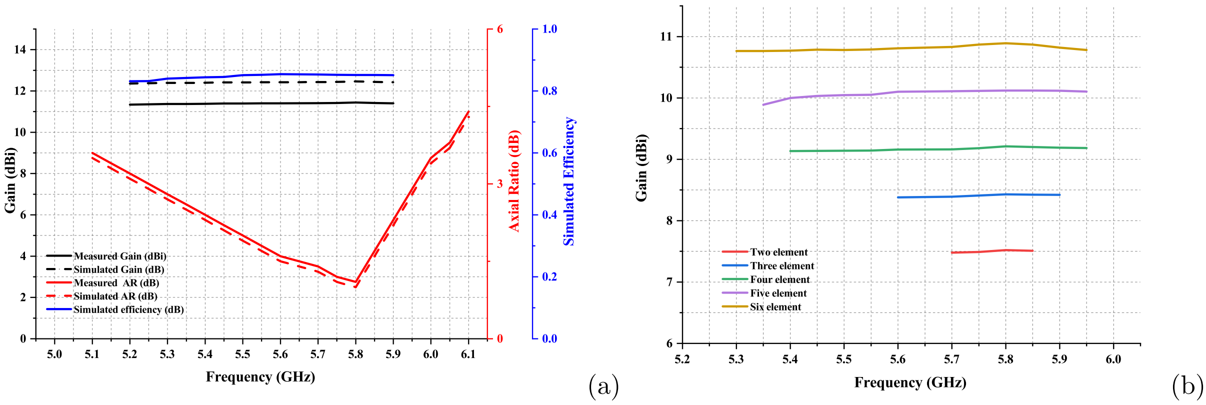

Fig. 20 (a) Simulated and measured boresight AR and gain of the antenna with terminating one of the ports; (b) Simulated gain for different array elements

- Conflict of interest: The authors declares that they have no conflict of interest to declare
- Ethics approval and consent to participate: not applicable
- Consent for publication: not applicable
- Data availability: all data are available within the manuscript
- Materials availability: not applicable
- Code availability: not applicable
- Author contribution: Writing - original draft preparation: [Yazeed Qasaymeh], Writing : [Mohammad Alibakhshikenari], Funding acquisition: [Omar Aharbi]; Resources: [Jaume Anguera], Methodology: [Isabelle Huynen], review: [Iyad Dayoub], editing: [Takfarinas Saber], review: [Ernesto Limiti], editing: [Abdullah Almuhaisen], review and editing

References

[1] Singhwal SS, Matekovits L, Peter I, Kanaujia BK (2022) A study on application of dielectric resonator antenna in implantable medical devices. IEEE Access 10:11846–11857. https://doi.org/10.1109/ACCESS.2022.3144664

[2] Raj A, Mandal D (2025) Design and Performance Analysis of Dielectric Resonator Antenna Array for 5G mm-Wave Ground-Based Navigation and Wireless Applications. Arab J Sci Eng 50:10611?10640. https://doi.org/10.1007/s13369-024-09745-5.

[3] Mukherjee B, Patel P, Mukherjee J (2019) A review of the recent advances in dielectric resonator antennas, Journal of Electromagnetic Waves and Applications 43(9):1095–1158. https://doi.org/10.1080/09205071.2020.1744484.

[4] Zhang B, Ren J, Sun X, Liu Y, Yin Y (2022) Four-port cylindrical pattern- and polarization-diversity dielectric resonator antenna for MIMO application. IEEE Trans. Antennas Propag 70(8): 7136–7141. https://doi.org/10.1109/TAP.2022.3145454.

[5] Rai JK, Ranjan P, Chowdhury R (2025) Dual-Band High Tuning Range Frequency Reconfigurable Cylindrical Dielectric Resonator Antenna for n7, n30, n38, n40, n41, n46, n47, n53 and n79 5G New Radio Application with Machine Learning Approach. Arab J Sci Eng 50:10555?10565. https://doi.org/10.1007/s13369-024-09684-1.

[6] Darimireddy NK, Reddy RR, Prasad AM (2018) Tri-band and quad-band dual L-slot coupled circularly polarized dielectric resonator antennas. International Journal of RF and Microwave Computer-Aided Engineering 28:1–13. https://doi.org/10.1002/mmce.21409.

[7] Ali M, Al-Hasan M, Mabrouk IB, Denidni TA (2022) Ultra-wideband hybrid magneto-electric dielectric-resonator dipole antenna fed by a printed RGW for millimeter-wave applications. IEEE Access 10:2028–2036. https://doi.org/10.1109/ACCESS.2021.3139828

[8] Yong-Xin G, Kwai-Man L (2018)Dual-polarized dielectric resonator antenna. IEEE Trans. Antennas Propag 51(5):1120–1123. https://doi.org/10.1002/mmce.21409.

[9] Thai-Van T , Trinh-Van S, Kang-Yoon L, Younggoo Y, and Keum C (2024) A Two-Port Dual-Band Dual-Circularly-Polarized Dielectric Resonator Antenna. Appl. Sci. 2024, 14(10), 4062. https://doi.org/10.3390/app14104062

[10] Ghatak R, Soren D, Mishra RK, Poddar DR (2012) Investigations on modified rectangular fractal curve shaped dielectric resonator antenna. International Journal of RF and Microwave Computer-Aided Engineering 22:394–401. https://doi.org/10.1002/mmce.20613.

[11] Zhong S, Kong LB, Tang XR (2014) Dual-polarized dielectric resonator antenna with very high isolation and lower cross-polarization. 2013 IEEE Antennas and Propagation Society International Symposium (APSURSI), Orlando, FL, USA, 2013, pp. 1242-1243, https://doi.org/10.1109/APS.2013.6711281 .

[12] Guo M, Yao F, Xuan WX, Zhong SS (2014) Broadband dual-polarized dielectric resonator antenna with high isolationa. 2014 IEEE Antennas and Propagation Society International Symposium (APSURSI), Memphis, TN, USA, 2014, pp. 1986-1987, https://doi.org/10.10.1109/APS.2014.6905320

[13] Sun YX, Leung KY (2013) Dual-band and wideband dual-polarized cylindrical dielectric resonator antennas. IEEE Antennas and Wireless Propagation Letters 12:384–387. https://doi.org/0.1109/LAWP.2013.2251993.

[14] Rana B, Parui SK (2015) Dual-polarized dielectric resonator antenna array. Microwave and Optical Technology Letters 58(1):24–27. https://doi.org/10.1002/mop.29539.

[15] Dwivedy B, Panigrahi A, Behera SK (2017) An enhanced gain dual-polarized dielectric resonator antenna array with high isolation for C-band applications. IETE Journal of Research 64(5): 602–611. https://doi.org/10.1080/03772063.2017.1367263.

[16] Kowalewski J, Jauch A, Eisenbeis J, Marahrens S, Disch K, Zwick T (2020) Dual-Polarized Dielectric Resonator Antenna Array for 5G Mobile Radio Base Stations. 2020 14th European Conference on Antennas and Propagation (EuCAP, Copenhagen, Denmark, pp. 1–4, https://doi.org/10.23919/EuCAP48036.2020.9135931

[17] El Yousfi A, Atia Abdalmalak K, Abdenasser L, Alejandro B, Bruno B, Segovia-Vargas D (2024) Miniaturized Dual-Polarized, High-Gain, and Wideband Dielectric Resonator Antenna for Low Band Massive MIMO Applications. Progress In Electromagnetics Research 179, 101-111. https://doi.org/10.2528/PIER24021303

[18] Fan W, Wu Q (2026) A Dual-Polarized Stacked Dielectric Resonator Antenna Array With Extremely Low Mutual Coupling for 6G Base Stations," in IEEE Transactions on Antennas and Propagation, vol. 74, no. 4, pp. 3035-3048, https://doi.org/10.1109/TAP.2026.3657177

[19] El Yousfi A, Atia Abdalmalak K, Abdenasser L, Alejandro B, Bruno B, Segovia-Vargas D. (2024) Miniaturized Dual-Polarized, High-Gain, and Wideband Dielectric Resonator Antenna for Low Band Massive MIMO Applications. Progress In Electromagnetics Research 179, 101-111. https://doi.org/10.2528/PIER24021303

[20] Pozar DM (1985)A microstrip antenna aperture coupled to a microstrip line. Electronics Letters 21(2):49-50. https://doi.org/10.1049/el:19850034.

[21] Kumar M, Singh SK, Singh AK, Tripurari S(2026) Octagonal-Shaped Super Wideband CPW-Fed Patch MIMO Antenna for Multiband Wireless Applications. J Infrared Milli Terahz Waves vol.47, no. 4 https://doi.org/10.1007/s10762-025-01109-w.

[22] Qasaymeh Y (2022) Compact interlaced dual circularly polarized sequentially rotated dielectric-resonator antenna array. Computers, Materials Continua 72(3): 4631–4643. https://doi.org/10.32604/cmc.2022.026111.

[23] Illahi U, Iqbal J, Irfan M, Sulaiman M, Khan M, Rauf A, Bari I, Abdullah M, Muhammad F, Nowakowski G, Glowacz A (2022) A Novel Design and Development of a Strip-Fed Circularly Polarized Rectangular Dielectric Resonator Antenna for 5G NR Sub-6 GHz Band Applications. Sensors 22(15):5531. https://doi.org/3390/s22155531.

[24] Mongia RK, Ittipiboon A (2017) Theoretical and experimental investigations on rectangular dielectric resonator antennas. Electromagnetics 37(1): 27–39. https://doi.org/10.1080/02726343.2017.1261222.

[25] Katiyar S, Yaduvanshi RS (2023) Tri-band high gain polarization reconfigurable split ring resonator based dielectric resonator antenna for terahertz applications. Optical and Quantum Electronics 55(972):1–22. https://doi.org/0.1007/s11082-023-05246-1.

[26] Bhakkiyalakshmi R, Vasanthi MS (2021) An octagonal ultra-wideband double slit antenna for WiMAX and WLAN rejection. Frequenz 76(1-2): 55–62. https://doi.org/10.1515/freq-2021-0068.

[27] Sharma N, Bhatia SS, Sharma V, Sivia JS (2019) An octagonal shaped monopole antenna for uwb applications with band notch characteristics. Wireless Personal Communications 111:1977–1997. https://doi.org/10.1007/s11277-019-06968-w.

[28] Eshrah A, Kishk AA, Yakovlev AB, Glisson AW (2005) Theory and implementation of dielectric resonator antenna excited by a waveguide slot. IEEE Transactions on Antennas and Propagation 53(1):483–494. https://doi.org/10.1007/s11277-019-06968-w.

[29] Bahl IJ, Prakash B (1980) Microstrip Antennas. Dedham, Mass, USA: Wadsworth.

[30] Cameron TR, Sutinjo AT, Okoniewski M (2010) A Circularly Polarized Broadside Radiating Herringbone Array Design With the Leaky-Wave Approach. IEEE Antennas and Wireless Propagation Letters 9: 26–29. https://doi.org/10.1109/LAWP.2010.2066950.

[31] Wang Y, Qu SW, Yang S (2022) Dual-polarized patch antenna array with hemispherical beam coverage. International Journal of RF and Microwave Computer-Aided Engineering 32(12):1–8. https://doi.org/10.1002/mmce.23460.

[32] GuoGuo SJ, Wu LS, Leung KW, Mao JF (2018) Microstrip-Fed Differential Dielectric Resonator Antenna and Array. IEEE Antennas and Wireless Propagation Letters 17(9): 1736–1739. https://doi.org/10.1109/LAWP.2018.2864972

[33] Sun K, Yang D, Chen Y, Liu A (2009) Analysis of traveling-wave-fed patch arrays. IEEE Transactions on Antennas and Propagation. 57(3): 664 –670. https://doi.org/10.1109/TAP.2009.2013434

[34] Min C, Free CE (2018) Analysis of traveling-wave-fed patch arrays. IEEE Transactions on Antennas and Propagation. 17(5):747–750. https://doi.org/10.1109/LAWP.2018.2813428.

[35] Yang YH, Guo IL, Sun BH, Cai YM, Zhou CGN (2018) The design of dual circularly polarized series-fed arrays. IEEE Transactions on Antennas and Propagation. 67(1):574–579. https://doi.org/10.1109/TAP.2018.2879775.

[36] Atanu C, Prashant R (2024) A Novel Stepped-Flower Shaped UWB Frequency Reconfigurable Printed Filtering Antenna Using PIN Diodes with Trackable Notch-Band for Mid-5G Band X-Band Applications. MAPAN. 39:1031–1044. https://doi.org/10.1007/s12647-024-00778-7.

[37] Atanu C, Prashant R (2023) A novel PIN diode-based frequency reconfigurable patch antenna with switching between the mid-5G and high-5G frequency band. International Journal of Microwave and Wireless Technologies. 16(1):595–604. https://doi.org/10.1017/S1759078723001149.

Table 1 Comparison between the proposed array and other DP DRA arrays reported in the literature

Reference **Size[mm^2]**	**DP technique**	**Polarization sense**	**Isolation Mechanism**	**Impedance bandwidth**	**Ports isolation [dB]**	**Gain[dBi]**
Rana and Parui (2016) [13] 135 ×85	Two differential orthogonal feds	DLP	within the DR boundary	5.34%	- 36	11.8
Dwivedy et al. (2018) [14] 190 ×82	Two differential feeding orthogonal ports	DLP	slot coupled mechanism	9.52%	- 15.8	12.5
Kowalewski et al. (2019) [15] 135 ×85	Two differential orthogonal feds	DLP	using slot coupled mechanism	5.34%	- 36	11.8
Yousfi et al (2024) [17] 100 ×100	Two differential orthogonal ports	DLP	within the DR boundary	13.3% for both ports	-17	7
Ma et al (2024) [18] 340 ×340	Two differential orthogonal ports	DLP	within the DR boundary	57.7% for both ports	-29.5	7
Fan et al (2026) [19] 60 ×60	Two differential orthogonal ports	DLP	within the DR boundary	16.49% for both ports	-17	5.7
proposed work	A traveling wave series-concentric ring fed coupling seven resonating elements each is composed of an octagonal slot coupling a	DCP	slot coupled mechanism	12.15% for both ports , 2.28% port 2	-39	12.4